ELSEVIER

International Journal of Heat and Fluid Flow 22 (2001) 19–29

International Journal of HEAT AND FLUID FLOW

www.elsevier.com/locate/ijhff

Towards the development of a Reynolds-averaged algebraic turbulent scalar-flux model

K. Abe [1], K. Suga *

Toyota Central Research and Development Labs., Inc., Nagakute, Aichi 480-1192, Japan

Received 26 February 1999; accepted 9 June 2000

Abstract

In order to derive a possible direction for developing Reynolds-averaged algebraic turbulent scalar-flux models, a priori explorations are attempted by processing the LES data presently performed for channel flows under several flow-boundary conditions including shear-free boundaries. The present calibration has elucidated that the turbulent scalar-flux vectors obtainable from the simple generalized gradient-diffusion hypothesis (GGDH) hardly align with the simulation results in wall-shear flows at $Pr \geqslant 0.71$. However, the GGDH form returns a quite reasonable approximation in shear-free flow regions and/or lower Pr fluid cases. In the former flow cases, it has been found that an introduction of quadratic products of the Reynolds-stress tensor into the gradient diffusion model may improve the predictive performance.

Keywords: Turbulent scalar transfer; Reynolds-stress tensor; Scalar-flux vector; Algebraic scalar-flux model; Gradient diffusion model

1. Introduction

Algebraic expressions for Reynolds-averaged turbulent scalar fluxes have been widely used in engineering applications since they provide mean scalar distributions with moderate satisfaction despite their simplicity. The most representative algebraic expression for turbulent scalar flux is based on the generalized gradient-diffusion hypothesis (GGDH) (Daly and Harlow, 1970). Although the GGDH model is useful, the crucial problem pointed out so far is that it gives an extreme underprediction of the streamwise scalar flux, $\overline{u\theta}$, compared with that in the wall-normal direction, $\overline{v\theta}$, even in simple wall-shear flows (Launder, 1976; Suga, 1995). To improve the model performance, many research groups have recently proposed more advanced algebraic models for the scalar fluxes (Nagano and Kim, 1988; Yoshizawa, 1988; Rogers et al., 1989; Nagano et al., 1991; Horiuti, 1992; So and Sommer, 1995; Abe et al., 1996; Rhee and Sung, 1997). Although these models gave encouraging results, there is still a wide margin to be improved. In order to predict each component of the scalar flux correctly, it is required in two-dimensional fields to obtain an accurate ratio of the components, $\overline{v\theta}/\overline{u\theta}$. In other words, the direction of the scalar-flux vector should be reproduced with sufficient accuracy.

Since it is rather difficult to reveal the turbulent scalar transport by experiments, many research groups have performed direct numerical simulation (DNS). The earliest example was done by Kim and Moin (1989), after that it was followed by Kasagi et al. (1991), Lyons et al. (1991) and so on, with different flow conditions. Among them, Kasagi and Nishimura (1997) discussed the principal axis of the Reynolds-stress tensor and the angle of the scalar-flux vector in some turbulent scalar fields. However, due to the excessive computational requirements of DNS, the investigated fluid Prandtl number is limited up to 5 (Kawamura et al., 1998). Furthermore, turbulent scalar fields near shear-free interfaces have been nearly unexplored.

Since the aim of the present study is to find a new way of Reynolds-averaged algebraic scalar-flux modeling, it is required to investigate a wide range of scalar field databases. Therefore, in this study, large eddy simulation (LES) of channel flows has been performed under several flow-boundary conditions and at several fluid Prandtl numbers, to make up the databases. Plane channel, open channel and the Couette–Poiseuille flows are chosen for the present test cases and the fluid Prandtl number ranges from 0.025 to 7. By processing the LES data, the present study carefully examines relations between the dynamic and scalar fields to derive a possible modeling way of Reynolds-averaged turbulent scalar fluxes in the context of algebraic models.

* Corresponding author. Tel.: +81-0561-63-4439; fax: +81-0561-63-6114.

E-mail address: suga@flow.tytlabs.co.jp (K. Suga).

[1] Present address: Department of Aeronautics and Astronautics, Kyushu University, Fukuoka 812-8581, Japan.

0142-727X/01/$ - see front matter
PII: S0142-727X(00)00062-X

Notation

h_j	subgrid-scale (SGS) scalar flux, $\langle U_j\Theta\rangle - \langle U_j\rangle\langle\Theta\rangle$
K_G	SGS turbulence energy, $\langle u'_i u'_i\rangle/2$
k	Reynolds-averaged (ensemble-averaged) turbulence energy, $\overline{u_i u_i}/2$
n	minimum distance from boundaries
n^*	nondimensional distance, $u_\varepsilon n/\nu$
$\langle P\rangle$	instantaneous filtered grid-scale (GS) pressure
Pr	molecular Prandtl number
Pr_{SGS}	SGS turbulent Prandtl number
Q_{in}	internal scalar source
$R_{u_i\theta}$	correlation coefficient of GS velocity fluctuation in i-direction and scalar fluctuation, $\overline{u_i\theta}/[(\overline{u_i^2})^{1/2}(\overline{\theta^2})^{1/2}]$
Re_τ	Reynolds number, $u_\tau\delta/\nu$
S_{ij}	GS strain-rate tensor, $\langle U_i\rangle_{,j} + \langle U_j\rangle_{,i}$
t	time
U_i	velocity in i-direction
$\langle U_i\rangle, u'_i$	instantaneous filtered GS velocity and SGS velocity fluctuation, $u'_i = U_i - \langle U_i\rangle$
$\overline{\langle U_i\rangle}, u_i$	ensemble-averaged GS velocity and its fluctuation, $u_i = \langle U_i\rangle - \overline{\langle U_i\rangle}$
u_ε	SGS Kolmogorov velocity scale, $(\nu\varepsilon_G)^{1/4}$
u_τ	mean friction coefficient on fixed wall
$\langle u'_i u'_j\rangle$	SGS Reynolds-stress tensor
$\overline{u_i u_j}$	Reynolds-averaged Reynolds-stress tensor
$\overline{u_i\theta}$	Reynolds-averaged scalar flux
u, v, w	u_1, u_2 and u_3
x, y, z	streamwise ($i = 1$), wall-normal ($i = 2$) and spanwise ($i = 3$) directions

Greeks

Δ	filter-width, $(\Delta_x\Delta_y\Delta_z)^{1/3}$
δ	representative length of channel flows
ε	dissipation rate of k
ε_G	dissipation rate of K_G
Θ	scalar
$\langle\Theta\rangle$	instantaneous filtered GS scalar
$\overline{\langle\Theta\rangle}, \theta$	ensemble-averaged GS scalar and its fluctuation, $\theta = \langle\Theta\rangle - \overline{\langle\Theta\rangle}$
ν, ν_{SGS}	kinematic and SGS eddy viscosities
ρ	fluid density
τ_{SGS}	SGS characteristic time scale
τ_{ij}	SGS stress, $\langle U_i U_j\rangle - \langle U_i\rangle\langle U_j\rangle$
Ω_{ij}	GS vorticity tensor, $\langle U_i\rangle_{,j} - \langle U_j\rangle_{,i}$

Special symbols

$f_{,i}$	partial derivative of variable, f, with respect to coordinate, x_i (e.g., $f_{,i} = \partial f/\partial x_i$)
$\overline{(\ )}$	ensemble-averaged value
$\langle(\ )\rangle$	volume-averaged value with filter-width Δ

2. LES

2.1. Governing equations and SGS model

The filtered governing equations of a dynamic field may be written as

$$\langle U_i\rangle_{,i} = 0, \tag{1}$$

$$\langle U_i\rangle_{,t} + \left(\langle U_i\rangle\langle U_j\rangle\right)_{,j} = -\frac{1}{\rho}\langle P\rangle_{,i} + \left\{\nu\left(\langle U_i\rangle_{,j} + \langle U_j\rangle_{,i}\right) - \tau_{ij}\right\}_{,j}, \tag{2}$$

where a quantity such as $\langle U_i\rangle$ is a volume-averaged value with the filter-width Δ. In the present study, the SGS stress, $\tau_{ij} = \langle U_i U_j\rangle - \langle U_i\rangle\langle U_j\rangle$, is approximated by the eddy-viscosity model (EVM) as

$$\tau^*_{ij} = \tau_{ij} - \frac{1}{3}\tau_{kk}\delta_{ij} = -\nu_{\mathrm{SGS}}\left(\langle U_i\rangle_{,j} + \langle U_j\rangle_{,i}\right), \tag{3}$$

where ν_{SGS} and τ^*_{ij} denote the SGS eddy viscosity and the anisotropic part of the SGS stress, respectively. The presently used SGS EVM is a one-equation SGS model (Schumann, 1975; Horiuti, 1985 etc.). In this approach, the SGS eddy viscosity is expressed as $\nu_{\mathrm{SGS}} = C\Delta K_G^{1/2}$ and the transport equation of K_G is modeled as

$$K_{G,t} + \left(\langle U_j\rangle K_G\right)_{,j} = \left\{(\nu + C_k K_G\tau_{\mathrm{SGS}})K_{G,j}\right\}_{,j} - \tau_{ij}\langle U_i\rangle_{,j} - \varepsilon_G, \tag{4}$$

where τ_{SGS} ($\propto \Delta/K_G^{1/2}$) is the SGS characteristic time scale.

Recently, Okamoto and Shima (1999) confirmed that the optimized constant C varies depending on the mean strain rate. They thus introduced a functional form of C to cover several kinds of flows, including a homogeneous decaying flow, a mixing layer, and channel flows with and without transpiration. Their form: $\nu_{\mathrm{SGS}} = C_\nu K_G^{1/2}\Delta/(1 + C_x\Delta^2 S_{mn}S_{mn}/K_G)$ was derived using the two-scale direct-interaction approximation (TSDIA) theory (Yoshizawa, 1991). They also fixed the near-wall inconsistency of the traditional form of $\varepsilon_G = C_\varepsilon K_G^{3/2}/\Delta$ by introducing a further term as

$$\varepsilon_G = C_\varepsilon\frac{K_G^{(3/2)}}{\Delta} + 2\nu\left(K_G^{(1/2)}\right)_{,j}\left(K_G^{(1/2)}\right)_{,j}. \tag{5}$$

The additional second term ensures the theoretical near-wall behavior of $K_G \propto y^2$, y being the direction normal to a no-slip wall surface.

Following their discussion, a functional form of ν_{SGS} similar to theirs but with an introduction of vorticity effects:

$$\nu_{\mathrm{SGS}} = \frac{C_\nu K_G^{(1/2)}\Delta}{1 + C_x\Delta^2(\alpha S_{mn}S_{mn} + \beta\Omega_{mn}\Omega_{mn})/K_G} \tag{6}$$

is presently employed. It may be rewritten by using $\tau_{\mathrm{SGS}} = C_\nu\Delta/K_G^{1/2}$ as

$$\nu_{\mathrm{SGS}} = \frac{K_G\tau_{\mathrm{SGS}}}{1 + (C_D\tau_{\mathrm{SGS}})^2(\alpha S_{mn}S_{mn} + \beta\Omega_{mn}\Omega_{mn})}, \tag{7}$$

where $C_\nu = C_\mu f_\mu$ and f_μ is the wall-damping function as described below. The theoretically obtained model constants by the TSDIA (Okamoto and Shima, 1999) are

$$C_\mu = 0.133,\quad (C_\mu C_D)^2\alpha = 0.039,\quad (C_\mu C_D)^2\beta = 0,\quad C_\mu C_K = 0.093,\quad C_\varepsilon = 0.92. \tag{8}$$

According to the present modification, the constants have been slightly retuned through the preliminary runs as

$$C_\mu = 0.12,\quad (C_\mu C_D)^2\alpha = 0.008,\quad (C_\mu C_D)^2\beta = 0.009,\quad C_\mu C_K = 0.1,\quad C_\varepsilon = 0.835. \tag{9}$$

The constants α and β are tuned to make the strain effects moderate though C_K and C_ε are kept the same as those of Okamoto and Shima (1999) (in fact, they also modified the theoretical values a little). Thus, the presently optimized set of coefficients is

$$C_\mu = 0.12, \quad C_D = 0.8, \quad \alpha = 5/6, \quad \beta = 1.0, \\ C_k = 0.833, \quad C_\varepsilon = 0.835. \tag{10}$$

When the SGS EVM is applied to wall-bounded flows, the eddy viscosity usually needs to be damped towards the wall unless the dynamic SGS approach (Germano et al., 1991) is adopted. Following Okamoto and Shima (1999), the present study then uses the van Driest type damping function with some modifications as

$$f_\mu = \left[1 - \exp\left\{-\left(\frac{n^*}{26}\right)^2\right\}\right], \tag{11}$$

$$n^* = \frac{u_\varepsilon n}{\nu}, \quad u_\varepsilon = (\nu \varepsilon_G)^{1/4}, \tag{12}$$

where n is the minimum distance from all boundaries in the flow field. Since the Kolmogorov scale, Eq. (12), does not vanish even at a shear-free point (Abe et al., 1994), its introduction instead of the wall-friction velocity is considered to be useful to avoid singularities in such shear-free flow regions. Note that as discussed by Ghosal et al. (1995), the realizability of K_G is not ensured with Eq. (4). We thus clipped K_G smaller than the prescribed value (1×10^{-12}) except on the walls to eliminate the negative value, though the case was not so frequently detected.

The filtered scalar-transport equation may be written as

$$\langle\Theta\rangle_{,t} + \left(\langle U_j\rangle\langle\Theta\rangle\right)_{,j} = \left\{\left(\frac{\nu}{Pr}\right)\langle\Theta\rangle_{,j} - h_j\right\}_{,j} + Q_{\mathrm{in}}, \tag{13}$$

where Q_{in} is an internal scalar source. The SGS scalar flux, $h_j = \langle U_j\Theta\rangle - \langle U_j\rangle\langle\Theta\rangle$, is also approximated by the eddy-viscosity model in the present study as

$$h_j = -\frac{\nu_{\mathrm{SGS}}}{Pr_{\mathrm{SGS}}}\langle\Theta\rangle_{,j}. \tag{14}$$

For the SGS scalar-flux modeling of Eq. (14), many workers have used $Pr_{\mathrm{SGS}} \sim 0.5$, however, a higher value may be desirable in a near-wall flow (e.g., Kawamura et al. (1994) used 0.83 to simulate the thermal field in a concentric annulus). In fact, Moin et al. (1991) reported that Pr_{SGS} varied from around 1.0 (near the wall) to about 0.5 (far from the wall). Therefore, the value of $Pr_{\mathrm{SGS}} = 0.9$ is applied in the present study since the reproduction of passive scalar phenomena in the buffer layer (i.e., the region around $y^+ \sim 20$ or less) is the most important issue in the LES of wall-bounded flow fields especially in medium and high Prandtl number cases.

According to the near-wall limiting behavior of the present SGS model ($K_G \propto y^2$, $f_\mu \propto y^2$ and $\nu_{\mathrm{SGS}} \propto y^3$), the correct near-wall behavior is obtained for τ_{12} and h_2. (The subscripts "1" and "2" denote the streamwise and wall-normal directions, respectively.) Although their limiting behavior near a free surface is not correct completely, the model has not provided any seriously unrealistic situation there.

Such being the case, the presently proposed SGS model solves some of the drawbacks of the original Smagorinsky SGS model pointed out by the previous workers. The model, however, has some margin to be discussed in more detail and further improved. But in this study, we focus on the Reynolds-averaged correlations obtainable from the LES rather than the SGS modeling.

The transport equations are discretized by the finite difference method on collocated grid systems. For all the spatial discretizations, the second-order central difference is used. As for the time integration of Eqs. (2), (4) and (13), the Crank–Nicholson implicit scheme is employed with the convection terms linearized.

2.2. Computational conditions

The simulations have been performed for fully developed channel flows with several flow-boundary conditions, which are listed in Table 1, including boundaries of a moving (almost shear-free) wall and a free surface. In these channel-flow calculations, the flow fields are assumed to be fully developed, and the periodic boundary condition is imposed in both the streamwise (x) and spanwise (z) directions. It is also assumed that there exists a mean scalar gradient only in the wall-normal (y) direction.

In Table 1, the codes, "W–W", "W–M" and "W–F", denote the boundary conditions for the velocity fields. For example, "W–F" means that one of the channel boundaries is a fixed wall and another is a free surface. As for the scalar field, "$Q_{\mathrm{in}} = 1$" is the Kim and Moin (1989) condition that imposes a constant scalar value on walls and an internal scalar source, while "$\Delta\Theta = 1$" indicates that there is a constant difference in the scalar values of the two boundaries. Note that, at the free surfaces of cases 11 and 12, the instantaneous local scalar flux is assumed to be constant, so that the scalar fluctuates there.

The no-slip boundary condition is adopted for the wall boundaries in all flow cases, so that the near-wall grid resolutions are carefully adjusted to resolve viscous sublayers.

Table 1
Computational conditions of channel flows[a]

Cases	Domain	Grid	Re_τ	Pr	B.C.	Resolution ($\Delta x^+, \Delta y^+, \Delta z^+$)	Time step (δ/u_τ)	Sampling time (δ/u_τ)
1, 2, 3, 4	$6.4\delta \times 2\delta \times 1.6\delta$	$64 \times 62 \times 64$	180	0.1, 0.71, 2, 7	W–W, $Q_{\mathrm{in}} = 1$	18, 0.5–14, 4.5	1×10^{-3}	30–48
5, 6, 7, 8, 9	$6.4\delta \times 2\delta \times 1.6\delta$	$64 \times 62 \times 64$	180	0.025, 0.1, 0.71, 2, 7	W–W, $\Delta\Theta = 1$	18, 0.5–14, 4.5	1×10^{-3}	27–49
10	$2.4\delta \times \delta \times 1.6\delta$	$64 \times 62 \times 64$	307	0.71	W–M, $\Delta\Theta = 1$	11.5, 0.5–8, 7.7	2×10^{-3}	102
11	$4.8\delta \times \delta \times 3.2\delta$	$64 \times 62 \times 64$	180	0.71	W–F, $\Delta\Theta = 1$	13.5, 0.4–5, 9	2×10^{-4}	26
12	$4.8\delta \times \delta \times 3.2\delta$	$92 \times 92 \times 80$	180	7	W–F, $\Delta\Theta = 1$	9.4, 0.1–4, 7.2	1×10^{-4}	12

[a] B.C.: Boundary condition, W: Fixed wall, M: Moving wall, F: Free surface.

3. Results and discussions

3.1. Validation of the LES

Results of the velocity-field calculations are compared with those of the corresponding DNSs (Kim and Moin, 1989; Kuroda et al., 1993; Lombardi et al., 1996) in Figs. 1–3. Note that all the shown turbulence statistics are GS quantities though the SGS contribution should be considered for the net comparison. However, since the ratio of K_{SGS} and the GS turbulence energy is always smaller than 3% in the present cases, the net comparisons should not have been so different from the presented figures. As seen in Figs. 1 and 2, the present mean velocity and Reynolds shear stress agree well with the DNS data. This indicates that the accuracy of the present LES is sufficiently enough for flow-field predictions of these cases. Although some discrepancies are seen in the distributions of turbulence intensities as shown in Fig. 3 (i.e., $(\overline{uu}^+)^{1/2}$ in cases 10 and 12 and $(\overline{ww}^+)^{1/2}$ in case 10), such slight errors give no serious effect on the following discussions.

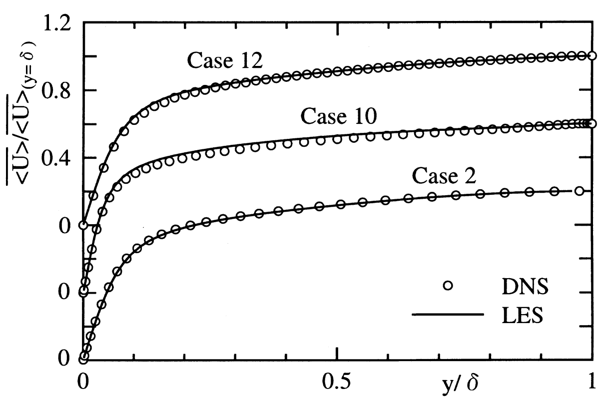

Fig. 1. Mean velocity profiless.

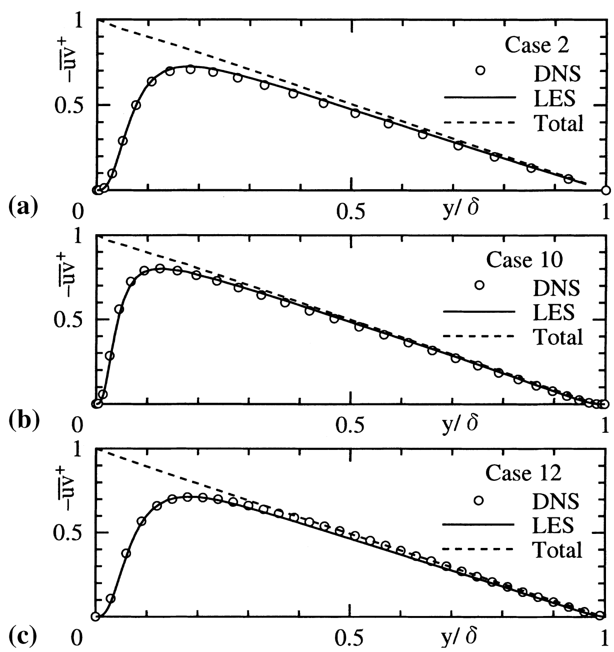

Fig. 2. Profiles of Reynolds shear stress.

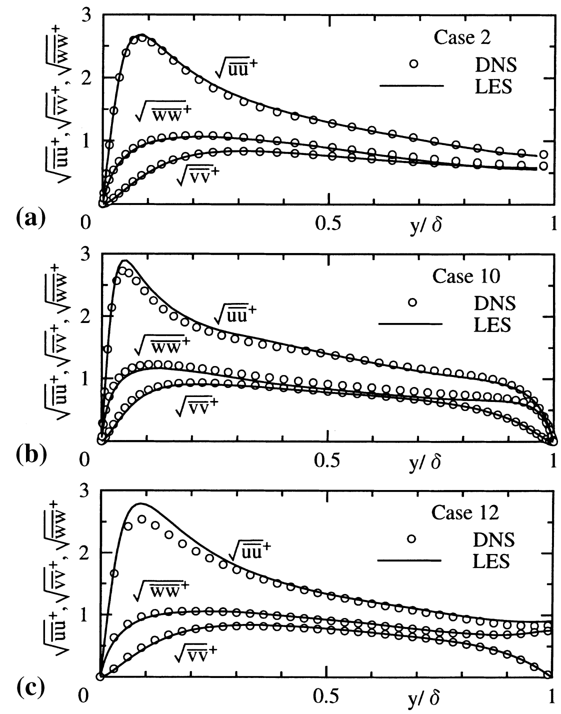

Fig. 3. Profiles of turbulence intensities.

Computational results of the mean scalar and scalar fluxes are shown in Figs. 4–6, where the DNS results of Kim and Moin (1989) are included for cases 1–3. As can be seen in Fig. 4, the mean scalar profiles of the present LES show excellent agreement with those of the corresponding DNS (Kim and Moin, 1989). As for the case of $Pr = 7$, the mean scalar prediction is also in good agreement with the experimental correlation of Kader (1981). Note that some upward shifts are seen in the mean scalar profiles of cases 6–9 (broken lines) compared with the corresponding experimental correlations. They are, however, caused by the difference between the scalar-boundary conditions of $Q_{in} = 1$ and $\Delta\Theta = 1$. Furthermore, as found in Figs. 5 and 6, the prediction accuracy of the scalar fluxes for cases 1–3 is also sufficient (the lines of the DNS results of cases 1 and 2 just overlap the LES results). Concerning the scalar-flux distributions of cases 10–12, we can see no serious problem which is in conflict with the specified flow-

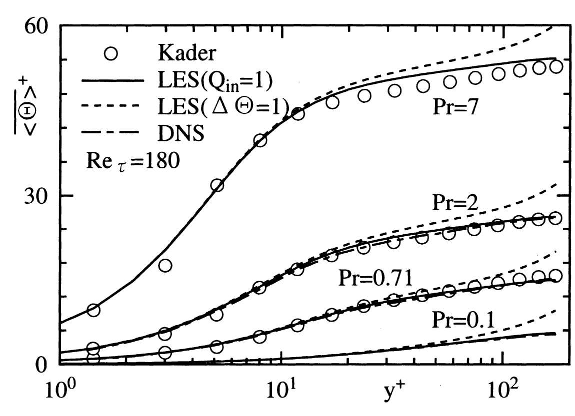

Fig. 4. Mean scalar profiles.

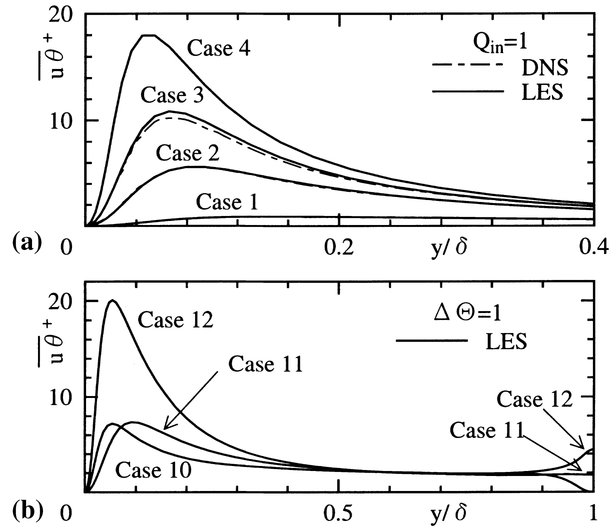

Fig. 5. Profiles of streamwise scalar flux.

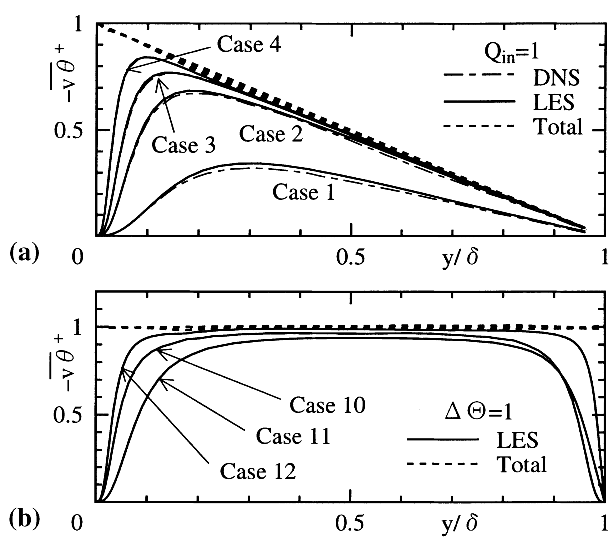

Fig. 6. Profiles of cross-streamwise scalar flux.

boundary conditions, although neither experimental nor DNS data is available for these cases.

Finally, it is confirmed from Figs. 2 and 6 that good numerical balances of the mean momentum and scalar transports are obtained only by the GS quantities, because the total shear-stress and scalar-flux profiles are reasonably straight although slight discrepancies are seen. This indicates that the grid resolutions presently used are fine enough to suitably minimize the effect of the SGS model on the reproduction of fundamental scalar-transport phenomena. Additional discussions on the grid dependency are presented in Appendix A to confirm the above discussions.

Nevertheless, a suspicion may arise on the present computational domain size. In fact, it is obvious that the presently employed domain size is not always adequately large, and thus some larger structure cannot be captured. However, the statistical results shown in Figs. 1–3 are reasonable and this implies that the contribution from such a large structure to the second moment quantities (which are required in the following section) is not very significant in the present cases.

From the aforementioned discussions, it is confirmed that the present LES results are sufficiently useful for the following discussions of the development of a Reynolds-averaged algebraic scalar-flux model.

3.2. Discussion of Reynolds-averaged scalar-flux models

Now, we focus on the discussion of the Reynolds-averaged scalar-flux modeling using the LES data.

Firstly, we consider the following GGDH model expression (Daly and Harlow, 1970), which is one of the simplest and has been often adopted in many engineering applications:

$$\overline{u_i\theta} = -C_\theta \tau_\theta \overline{u_i u_j}\,\overline{\Theta}_{,j}, \tag{15}$$

where C_θ and τ_θ are a model coefficient and a characteristic time scale, respectively. As pointed out by Kim and Moin (1989), θ in the wall-shear region correlates more strongly with u than with v. Kim and Moin (1989) thus suggested that it might be an interesting attempt to model the scalar fluxes, $\overline{u\theta}$ and $\overline{v\theta}$, using the Reynolds stresses, $\overline{uu}$ and $\overline{uv}$, since the following relation is expected to be held:

$$\overline{u\theta} \propto \overline{uu}, \quad \overline{v\theta} \propto \overline{vu}\ (\propto \overline{uv}). \tag{16}$$

As an estimation of the model performance, distributions of the model coefficient C_θ in case 2 are shown in Fig. 7, where τ_θ is defined as k/ε and C_θ is calculated by Eq. (15) in the x- and y-directions, respectively. As seen in the figure, C_θ for $\overline{v\theta}$ (i.e., in the y-direction) globally shows a constant value of about 0.3, except for the near-wall region of $x/\delta < 0.1$. However, C_θ for $\overline{u\theta}$ (i.e., in the x-direction) is more than three times as large as that for $\overline{v\theta}$. This indicates that it is impossible to satisfactorily predict both components of the scalar-flux vector by using Eq. (15) with a single coefficient of C_θ. In case that the mean scalar gradient exists only in the y-direction, the following relation between the scalar fluxes can be obtained from Eq. (15):

$$\frac{\overline{v\theta}}{\overline{u\theta}} = \frac{\overline{vv}}{\overline{uv}}. \tag{17}$$

Consequently, Eq. (17) suggests that the ratio of the scalar-flux components is not consistent with that implied by Eq. (16), i.e., $\overline{v\theta}/\overline{u\theta} = \overline{uv}/\overline{uu}$. This is the main reason why the GGDH form cannot successfully predict the streamwise scalar flux as pointed out previously (Launder, 1976; Suga, 1995), since the flux ratio directly connects with the direction of the flux vector. (When a model is constructed to give reasonable $\overline{v\theta}$ only, the level of $\overline{u\theta}$ is not necessarily reasonable without a correct ratio of the fluxes.)

With this in mind, in order to reflect the relation of Eq. (16) more precisely, the present study has investigated the following tensor expression as an extended version:

$$\overline{u_i\theta} = -C_\theta \tau_\theta \overline{u_i u_k} A_{kj} \overline{\Theta}_{,j}, \tag{18}$$

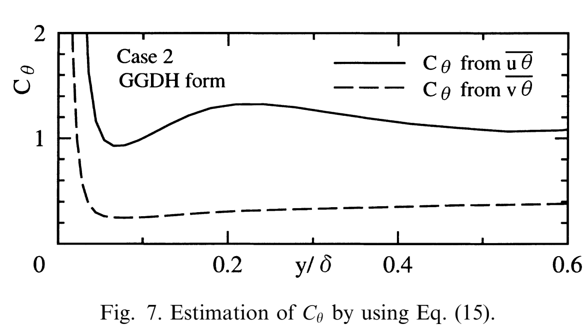

Fig. 7. Estimation of C_θ by using Eq. (15).

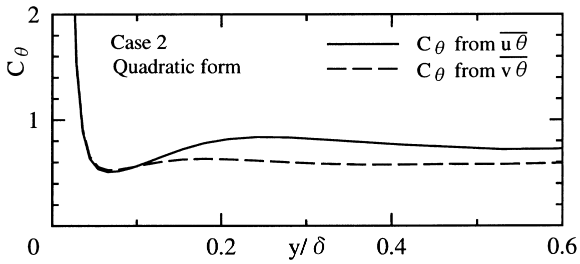

Fig. 8. Estimation of C_θ by using Eq. (19).

where A_{ij} is a nondimensional tensor. As for the modeling of A_{ij}, $A_{12} \neq 0$ is needed to reflect the relation of Eq. (16) and it is, of course, reasonable that A_{ij} is composed of physically appropriate quantities of turbulence. In this sense, for example, the strain-rate, the vorticity and the Reynolds-stress tensors can be considered in modeling A_{ij}. Considering this, the present study introduces the normalized Reynolds-stress tensor, $\overline{u_i u_j}/k$, as A_{ij}:

$$\overline{u_i\theta} = -C_\theta \tau_\theta \left(\frac{\overline{u_i u_k}\,\overline{u_k u_j}}{k} \right) \overline{\Theta}_{,j}. \tag{19}$$

This is regarded as a higher order extension of the GGDH form by using the quadratic products of the Reynolds-stress tensor (hereinafter referred to as the quadratic form). In case only $\overline{\Theta}_{,y}$ exists, the following relation is derived from Eq. (19):

$$\frac{\overline{v\theta}}{\overline{u\theta}} = \frac{\overline{uv}^2 + \overline{vv}^2}{(\overline{uu} + \overline{vv})\overline{uv}} \to \frac{\overline{uv}}{\overline{uu}} \quad \text{(near a wall)}. \tag{20}$$

The ratio: $\overline{v\theta}/\overline{u\theta}$ becomes nearly $\overline{uv}/\overline{uu}$ in the near-wall region under high shear strain and thus the quadratic form gives an answer for the above discussion.

Fig. 8 compares distributions of the model coefficient C_θ in case 2 calculated by the quadratic form. In contrast to Fig. 7, distributions of C_θ in both the x- and y-directions show nearly the same tendency. In the vicinity of the wall, the profiles of C_θ show almost the same value at the same location. This is a notable feature of the quadratic form and it indicates that the direction of the scalar-flux vector can be predicted by the quadratic form much more precisely, at least for this case.

3.3. A priori estimation in the channel flows

In what follows, the predictive performance of the GGDH (Eq. (15)) and the quadratic (Eq. (19)) forms is estimated by a priori tests using the present LES data, focusing especially on the directions of the scalar-flux vector. In Figs. 9 and 10, the distributions of the scalar-flux vector angles predicted by the GGDH and the quadratic forms for cases 5–9 are compared with those by the LES. The correlation coefficients and the angle of the principal axis of the Reynolds-stress tensor obtained from the LES are also shown in the figures. As seen in Fig. 9(a), the vector angle by the quadratic form is much closer to that of the LES compared with that of the GGDH at $Pr \geqslant 0.71$. It is also found that the profile of the scalar-flux vector angle by the LES does not change greatly with the increase of Pr in the range of $Pr \geqslant 0.71$ (hereinafter referred to as the higher Pr cases for convenience). On the other hand, as found from Fig. 10(a), the profile of the scalar-flux vector angle becomes closer to that by the GGDH in the lower Pr cases. The distributions of the correlation coefficients as shown in Figs. 9 and 10 correspond to these features. In the higher Pr cases shown in Fig. 9(b) and (c), θ correlates strongly with u, as pointed out previously. However, as seen in Fig. 10(b) and (c),

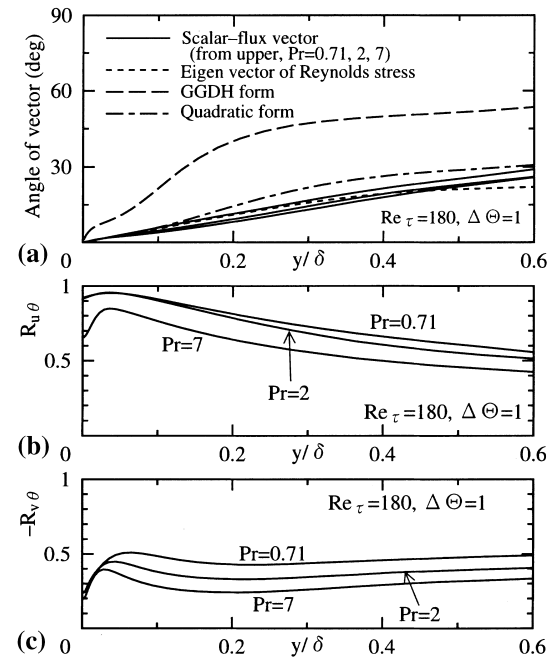

Fig. 9. Estimation of angle of vectors and correlation coefficients (cases 7–9).

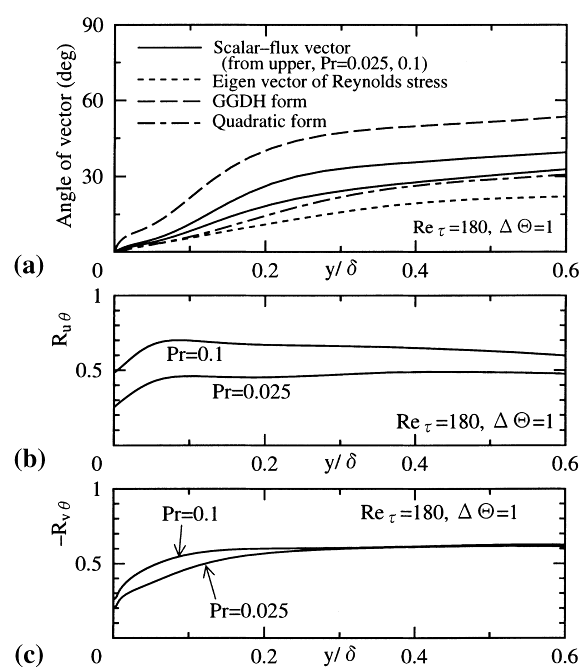

Fig. 10. Estimation of angle of vectors and correlation coefficients (cases 5 and 6).

the correlation between θ and v relatively increases with the decrease of Pr, and then it becomes almost the same level as that between θ and u in case of $Pr = 0.025$. Consequently, for predicting the scalar-flux vector angle, some Prandtl-number dependence should be considered especially in the lower Pr cases, whereas it is not always the primary issue in wall-shear flows at high Pr.

The results of the Couette–Poiseuille (case 10) and the open channel (cases 11 and 12) flows estimated in the same manner as above are shown in Figs. 11 and 12, respectively. In the shear-free regions near the location of $x/\delta = 1$, the GGDH form is a reasonably better approximation irrespective of the Prandtl number, in contrast to the wall-shear regions. As seen in Figs. 11(b) and 12(b), near the shear-free regions, the level of the correlation coefficient between θ and v is globally equal to that between θ and u. Moreover, on the moving wall of case 10, the correlation between θ and u almost vanishes. These suggest that it is difficult to predict the scalar-flux vector angle accurately for various kinds of scalar-transfer fields by using a single expression of the GGDH or the quadratic form.

In order to compare the performance of the models presently and previously proposed, the same estimation of the model of Rogers et al. (1989) is shown in Fig. 13. Most previous "explicit" algebraic models introduced some effects of the mean strain rate into the model expressions (Yoshizawa, 1988; Rogers et al., 1989; Horiuti, 1992; So and Sommer, 1995; Abe et al., 1996; Rhee and Sung, 1997). Such an extension may

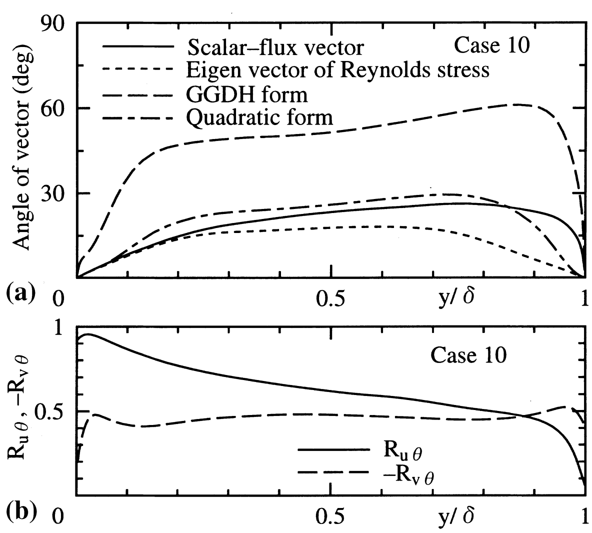

Fig. 11. Estimation of angle of vectors and correlation coefficients (case 10).

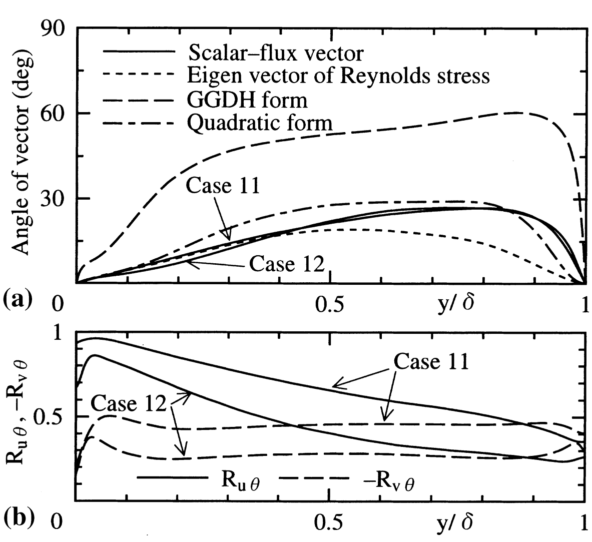

Fig. 12. Estimation of angle of vectors and correlation coefficients (cases 11 and 12).

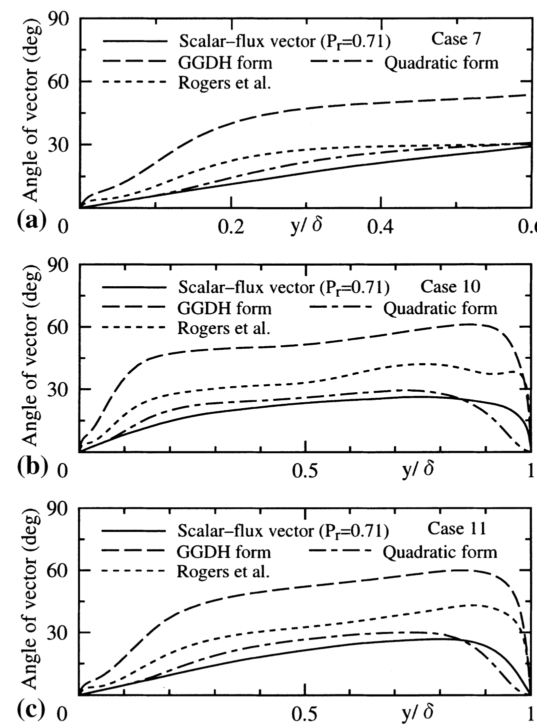

Fig. 13. Estimation of angle of vectors and correlation coefficients (comparison with the previous work of Rogers et al. (1989)).

be an effective modeling way because it is directly expected from the relation between algebraic and scalar-flux transport models. As seen in Fig. 13, however, the model performance of Rogers et al. (1989) is not so good as that of the quadratic form. It is noted that considerable discrepancies can be seen between the results of the Rogers et al.'s model and the LES data even in the near shear-wall regions. When this kind of model expressions were derived, a simple linearized model of the pressure-scalar gradient correlation was usually considered. This may be the main reason why the previous models cannot successfully predict the scalar-flux vector angles. However, nonlinear extensions of the pressure-scalar gradient correlation prevent us from deriving such an explicit algebraic model. (Note that the present discussion does not deny the potential of introducing the mean strain-rate effects.)

3.4. Estimation in some other flows

To investigate further applicability of the present proposal, the GGDH and the quadratic forms are applied to the Sumitani and Kasagi (1995) channel flow with wall injection and suction, and the Tavoularis and Corrsin (1981) homogeneous shear flow. Fig. 14 compares the distributions of the angles of the scalar-flux vectors obtained from the DNS and the experimental data. It is readily seen that the vector angle of the quadratic form correlates very well with the DNS even in the regions with wall injection and suction. Furthermore, as seen in Fig. 14(c), the vector angle of the quadratic form is very close to the experimental one in the homogeneous shear flow. This indicates that the quadratic form is effective in predicting the scalar-transport phenomena in a wide range of flow fields under high shear strain, regardless of the existence of a wall.

In sum, taking account of the above discussions, in order to construct a new algebraic scalar-flux model applicable to various kinds of scalar-transfer fields, a combined expression

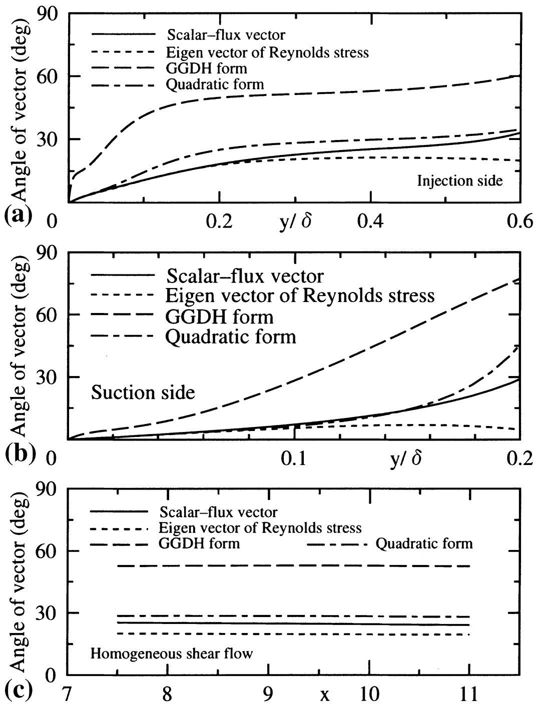

Fig. 14. Estimation of angle of vectors: (a) DNS (Sumitani and Kasagi, 1995), injection side; (b) DNS (Sumitani and Kasagi, 1995), suction side; (c) homogeneous shear flow (Tavoularis and Corrsin, 1981).

of the GGDH and the quadratic forms is considered to be effective. It may be written as

$$\overline{u_i\theta} = -k\tau_\theta\left(C_{\theta 1}\frac{\overline{u_iu_j}}{k} + C_{\theta 2}\frac{\overline{u_iu_k}\,\overline{u_ku_j}}{k^2}\right)\overline{\Theta}_{,j}, \tag{21}$$

where $C_{\theta 1}$ and $C_{\theta 2}$ are model coefficients. The functional coefficients: $C_{\theta 1}$ and $C_{\theta 2}$, are to be modeled so that the second term in the right-hand side of Eq. (21) plays the most dominant role under high shear strain, while the first term mainly works in situations under weak shear strain as well as in lower *Pr* flow cases.

Note that the assessment of the applicability of the model: Eq. (21) to the turbulent diffusion in the k-equation is presented in Appendix B.

4. Concluding remarks

LES simulations of channel flows with a wall-normal temperature gradient have been performed under several flow-boundary conditions and at several fluid Prandtl numbers. By processing the LES data, the present study carefully examines relations between the dynamic and scalar fields to derive a possible modeling way of Reynolds-averaged turbulent scalar fluxes in the context of algebraic models. The following are the main contributions obtained from the present study:

- A priori tests of the channel-flow cases elucidate that the Reynolds-averaged turbulent scalar-flux vectors predicted by the GGDH form hardly align with the simulation results in wall-shear regions at $Pr \geqslant 0.71$.
- In the above situations, the introduction of quadratic products of the Reynolds-stress tensor into the gradient-diffusion model, i.e., the quadratic form, shows its potential to improve the prediction accuracy.
- The quadratic form is useful in predicting turbulent scalar transfer in a channel flow with wall injection and suction. Moreover, it is also effective in a homogeneous shear flow. This indicates that the quadratic form is effective in predicting the scalar-transport phenomena in a wide range of flow fields under high shear strain, regardless of the existence of a wall.
- On the other hand, the GGDH form returns a quite reasonable approximation for scalar-flux vectors in shear-free boundary layers and lower *Pr* flows.
- In order to construct a new algebraic scalar-flux model applicable to various kinds of Reynolds-averaged scalar-transfer fields, a combined model expression of both the GGDH and the quadratic forms is recommended, although further discussions on finding functional coefficients are needed.

Acknowledgements

The authors wish to express their appreciation to Mr. M. Inagaki of TCRDL for his help and suggestion in developing the computer program used in the present study.

Appendix A. Quality of the present LES

In order to more carefully examine the quality of the present LES data for deriving the main conclusions of the paper, the discussion on the grid dependency of the LES data is presented. In Figs. 15–17, the present LES results are compared with those by using coarser grids, where the number of grid points is $32 \times 62 \times 32$ (hereinafter referred to as the coarser grid cases for convenience). As seen in the figures, the mean velocity and scalar distributions of the coarser grid cases show good agreement with those of the present LES data, while some grid dependency is seen in the statistical second moments. Fig. 18 compares the results of the vector angles calculated by the LES data of the coarser grid cases. From this

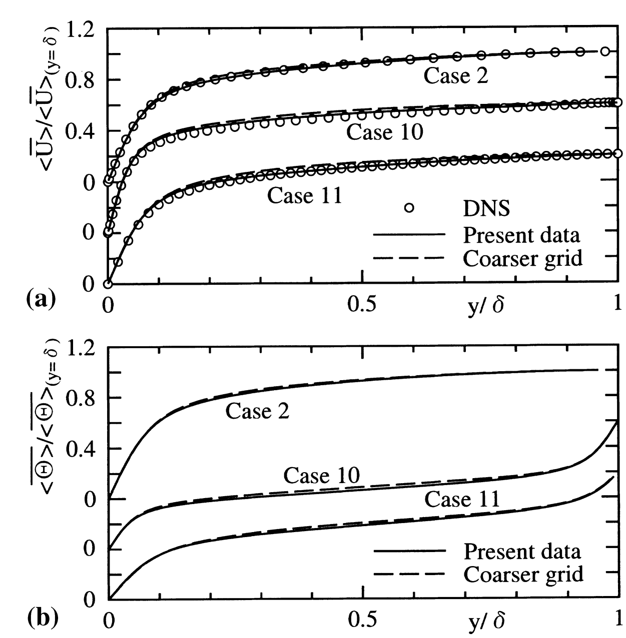

Fig. 15. Estimation of grid dependency for mean velocity and mean scalar of channel-flow cases.

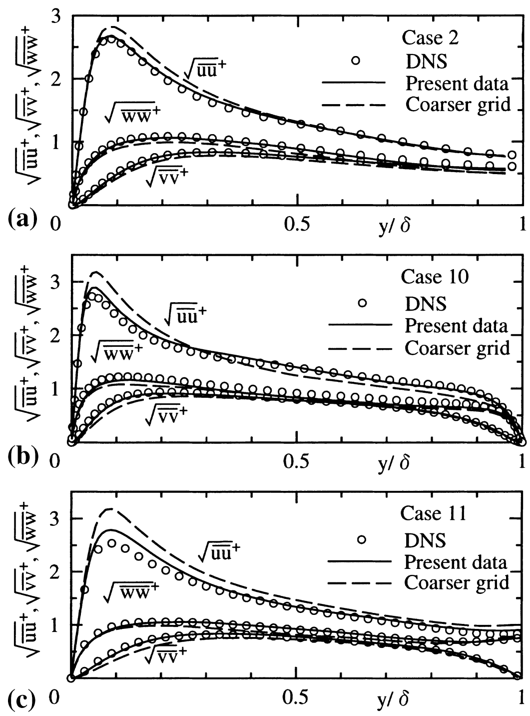

Fig. 16. Estimation of grid dependency for turbulent velocity statistics of channel-flow cases.

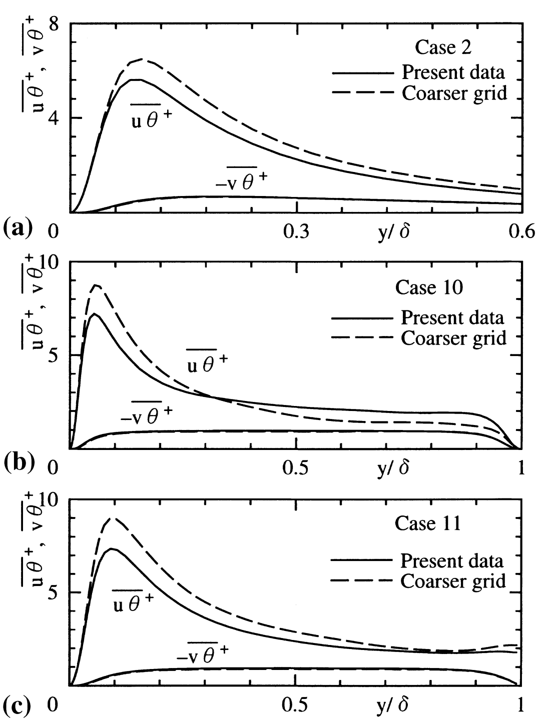

Fig. 17. Estimation of grid dependency for turbulent scalar statistics of channel-flow cases.

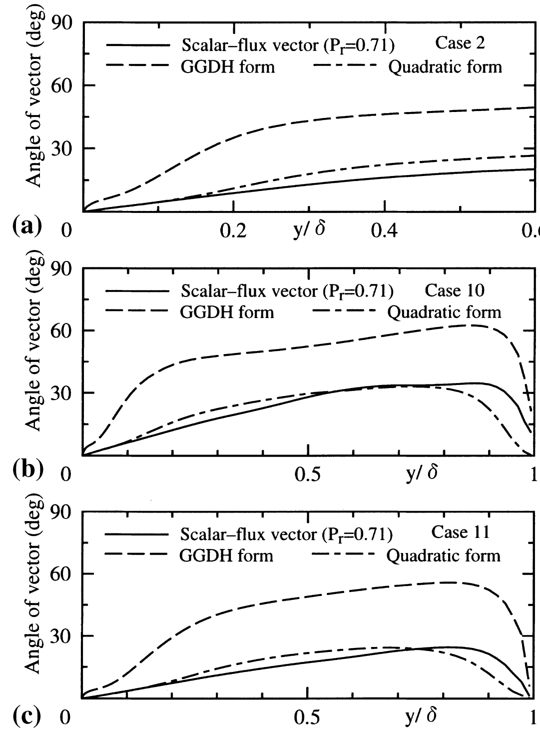

Fig. 18. Estimation of angle of vectors in coarser grid cases.

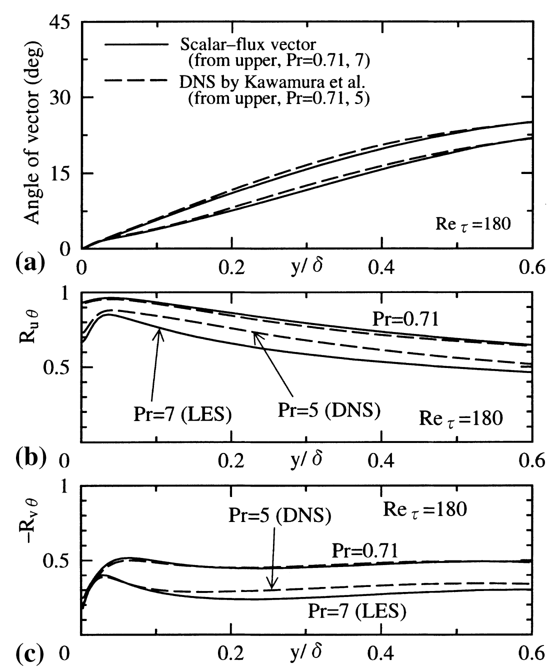

Fig. 19. Comparisons with the DNS by Kawamura et al. (1998).

figure, it should be noted that the estimations of vector-angle distributions in the coarser grid cases show almost the same tendency as those shown in Figs. 9, 11 and 12. This is important because the fact also implies that the same conclusions as in the present study can be drawn even with much finer grids. In other words, this indicates that the present LES data have successfully captured fundamental turbulent structures dominating the passive scalar transfer in the fields, though they may still have some local grid dependency.

Comparisons of the present LES results with those of the DNS by Kawamura et al. (1998) are shown in Fig. 19. Note that the computational conditions of the DNS by Kawamura et al. (1998) are slightly different from those of the present

LES. The DNS adopts a constant scalar-flux boundary condition and a slightly lower value of $Pr = 5$ is selected in the higher Pr case. The predicted vector angles of the present LES show almost the same tendency as those of the DNS, as seen in Fig. 19(a). Fig. 19(b) and (c) compares the correlation coefficients. Since the discrepancies found in the figures mainly come from the differences in the Prandtl number and the boundary condition, it is confirmed that the present results of $Pr = 7$ do not produce any inconsistency with the DNS of $Pr = 5$. This implies that the essential Prandtl number effects are successfully reproduced, though the numerical error according to the grid resolution is reasonably considered not to be very small in the higher Pr cases.

Appendix B. Modeling the turbulent diffusion vector

Modeling turbulent diffusion processes is another important matter from the engineering viewpoint (Hanjalic, 1994; Kawamura et al., 1995). Therefore, to assess the capability of the present proposal, Fig. 20 compares vector angles of the turbulent diffusion of the k-equation (i.e., $\overline{u_i(u_k u_k/2)}$), the scalar-flux ($\overline{u_i\theta}$) and the aforementioned model expressions. As seen in the figure, vector angles of the turbulent diffusion correlate well with those of the scalar flux and thus those of the quadratic form in the wall-shear regions. (Some kinks are seen in the turbulent diffusion vector-angle profiles in the proximity of the wall. They correspond to changes of the sign of the wall-normal turbulent diffusion.) Hence, the fluctuating part of turbulence energy $(u_k u_k/2)$ is considered to be transported by a mechanism similar to that of the passive scalar (θ) in wall-shear regions. Interestingly, even in the shear-free regions, the vector angles of the turbulent diffusion are rather close to those of the quadratic form. This is one of the key factors to model the turbulent diffusion phenomena successfully. However, considering the fact that the turbulent diffusion vector is originally derived from the triple moment tensor of the velocity fluctuations, one may need more careful and detailed discussions.

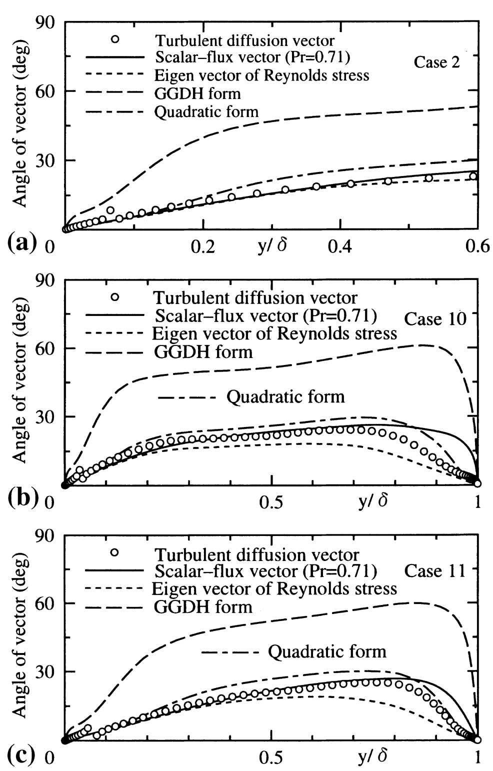

Fig. 20. Estimation of angle of vectors for turbulent diffusion.

References

Abe, K., Kondoh, T., Nagano, Y., 1994. A new turbulence model for predicting fluid flow and heat transfer in separating and reattaching flows – I. Flow field calculations. Int. J. Heat Mass Transfer 37, 139–151.

Abe, K., Kondoh, T., Nagano, Y., 1996. A two-equation heat transfer model reflecting second-moment closures for wall and free turbulent flows. Int. J. Heat Fluid Flow 17, 228–237.

Daly, B.J., Harlow, F.H., 1970. Transport equations in turbulence. Phys. Fluids 13, 2634–2649.

Germano, M., Piomelli, U., Moin, P., Cabot, W.H., 1991. A dynamic subgrid-scale eddy viscosity model. Phys. Fluids A 3, 1760–1764.

Ghosal, S., Lund, T., Moin, P., Akselvoll, K., 1995. A dynamic localization model for large-eddy simulation of turbulent flows. J. Fluid Mech. 286, 229–255.

Hanjalic, K., 1994. Advanced turbulence closure models: a view of current status and future prospects. Int. J. Heat Fluid Flow 15, 178–203.

Horiuti, K., 1985. Large eddy simulation of turbulent channel flow by one-equation modeling. J. Phys. Soc. Jpn. 584, 2855–2865.

Horiuti, K., 1992. Assessment of two-equation models of turbulent passive-scalar diffusion in channel flow. J. Fluid Mech. 238, 405–433.

Kader, B.A., 1981. Temperature and concentration profiles in fully turbulent boundary layers. Int. J. Heat Mass Transfer 24, 1541–1544.

Kasagi, N., Tomita, Y., Kuroda, A., 1991. Direct numerical simulation of the passive scalar field in a two-dimensional turbulent channel flow. ASME/JSME Thermal Eng. Proc. 3, 175–182.

Kasagi, N., Nishimura, M., 1997. Direct numerical simulation of combined forced and natural turbulent convection in a vertical plane channel. Int. J. Heat Fluid Flow 18, 88–99.

Kawamura, H., Nakamura, S., Satake, S., Kunugi, T., 1994. Large eddy simulation of turbulent heat transfer in a concentric annulus. Thermal Sci. Eng. 2 (2), 16–25.

Kawamura, H., Sasaki, J., Kobayashi, K., 1995. Budget and modelling of triple-moment velocity correlations in a turbulent channel flow based on DNS. In: Proceedings of the 10th Symposium on Turbulent Shear Flows, Penn State, pp. 26.13–26.18.

Kawamura, H., Ohsaka, K., Abe, H., Yamamoto, K., 1998. DNS of turbulent heat transfer in channel flow with low to medium-high Prandtl number fluid. Int. J. Heat Fluid Flow 19, 482–491.

Kim, J., Moin, P., 1989. Transport of passive scalars in a turbulent channel flows. Turbulent Shear Flows, vol. 6. Springer, Berlin, pp. 85–96 .

Kuroda, A., Kasagi, N., Hirata, M., 1993. Direct numerical simulation of turbulent plane Couette–Poiseuille flows: effect of mean shear on the near wall turbulence structures. In: Proceedings of the Nineth Symposium on Turbulent Shear Flows, Kyoto, pp. 8.4.1–8.4.6.

Launder, B.E., 1976. Turbulence. In: Bradshaw, P. (Ed.), Springer, Berlin, pp. 231–287.

Lombardi, P., Angelis, V.D., Banerjee, S., 1996. Direct numerical simulation of near-interface turbulence in coupled gas-liquid flow. Phys. Fluids 8, 1643–1665.

Lyons, S.L., Hanratty, T.J., Mclaughlin, J.B., 1991. Direct numerical simulation of passive heat transfer in a turbulent channel flow. Int. J. Heat Mass Transfer 34, 1149–1161.

Moin, P., Squires, K., Cabot, W., Lee, S., 1991. A dynamic subgrid-scale model for compressible turbulence and scalar transport. Phys. Fluids A 3, 2746–2757.

Nagano, Y., Kim, C., 1988. A two-equation model for heat transport in wall turbulent shear flows. Trans. ASME: J. Heat Transfer 110, 583–589.

Nagano, Y., Tagawa, M., Tsuji, T., 1991. An improved two-equation heat transfer model for wall turbulent shear flows. ASME/JSME Thermal Eng. Proc. 3, 233–240.

Okamoto, M., Shima, N., 1999. Investigation for the one-equation-type subgrid model with eddy-viscosity expression including the shear-damping effect. JSME Int. J. Ser. B 42, 154–161.

Rhee, G.H., Sung, H.J., 1997. A low-Reynolds-number, four-equation heat transfer model for turbulent separated and reattaching flows. Int. J. Heat Fluid Flow 18, 38–44.

Rogers, M.M., Mansour, N., Reynolds, W.C., 1989. An algebraic model for the turbulent flux of a passive scalar. J. Fluid Mech. 203, 77–101.

Schumann, U., 1975. Subgrid scale model for finite difference simulations of turbulent flows in plane channels and annuli. J. Comput. Phys. 18, 376–404.

So, R.M.C., Sommer, T.P., 1995. An explicit algebraic heat-flux model for the temperature field. Int. J. Heat Mass Transfer 39, 455–465.

Suga, K., 1995. Development and application of a non-linear eddy viscosity model sensitized to stress and strain invariants. Ph.D Thesis (UMIST).

Sumitani, Y., Kasagi, N., 1995. Direct numerical simulation of turbulent transport with uniform wall injection and suction. AIAA J. 33, 1220–1228.

Tavoularis, S., Corrsin, S., 1981. Experiments in nearly homogeneous turbulent shear flow with a uniform mean temperature gradient. Part I.. J. Fluid Mech. 104, 311–347.

Yoshizawa, A., 1988. Statistical modelling of passive-scalar diffusion in turbulent shear flows. J. Fluid Mech. 195, 541–555.

Yoshizawa, A., 1991. Eddy-viscosity-type subgrid-scale model with a variable Smagorinsky coefficient and its relationship with the one-equation model in large eddy simulation. Phys. Fluids A 3, 2007–2009.